Log Nr. 091

DESIGN AND ANALYSIS OF RTGs FOR CRAF AND CASSINI MISSIONS

Alfred Schock, Heros Noravian, Chuen Or, and Kumar Sankaranakandath
Fairchild Space
20301 Century Blvd.
Germantown, MD 20874
(301) 428-6272

MANUSCRIPT prepared for:

Eighth Symposium
on Space Nuclear Power Systems
Albuquerque, New Mexico
7-10 January 1991

Address all correspondence to: Mr. Alfred Schock

The work summarized in this paper was supported by the U.S. Department of Energy, Office of Special Applications.

DESIGN AND ANALYSIS OF RTGs FOR CRAF AND CASSINI MISSIONS

A. Schock (Author and Principal Investigator)
H. Noravian, T. Or, V. Sankarankandath (Contributors)

Fairchild Space
Germantown, Maryland 20874 U.S.A.

ABSTRACT

The design and analysis of Radioisotope Thermoelectric Generators integrated with JPL's CRAF and Cassini spacecraft are described. The principal purposes of the CRAF mission are the study of asteroids and comets, and the principal purposes of the Cassini mission are the study of asteroids, Saturn, and its moons (particularly Titan). Both missions will employ the Mariner/Mark-2 spacecraft, and each will be powered by two GPHS-RTGs. JPL's spacecraft designers wish to locate the two RTGs in close proximity to each other, resulting in mutual and unsymmetrical obstruction of their heat rejection paths. To support JPL's design studies, the U.S. Department of Energy asked Fairchild to determine the effect of the RTGs' proximity on their power output. This required the development of novel analysis methods and computer codes, described in this paper for the coupled thermal and electrical analysis of obstructed RTGs with axial and circumferential temperature, voltage, and current variations. The code was validated against measured data of unobstructed RTG tests, and was used for the detailed analysis of the obstructed CRAF/Cassini RTGs. Also described is a new method for predicting the combined effect of fuel decay and thermoelectric degradation on the output of obstructed RTGs, which accounts for the effect of diminishing temperatures on degradation rates. The computed results indicate that for the 24-degree separation angle of JPL's baseline design, the mutually obstructed standard GPHS/RTGs show adequate power margins for the CRAF mission, but slightly negative margins for the Cassini mission.

INTRODUCTION

The Jet Propulsion Laboratory (JPL) is in the process of designing spacecraft for NASA's upcoming CRAF and Cassini missions [1]. The CRAF (Comet Rendezvous and Asteroid Flyby) spacecraft, which is scheduled for a 1995 launch, will fly by at least one asteroid, orbit a comet, and launch an instrumented penetrator/lander into the comet's nucleus. The Cassini spacecraft, scheduled for a 1996 launch, will also fly by at least one asteroid, fly by Jupiter, orbit the planet Saturn, repeatedly fly by a number of Saturn's moons, and send an instrumented probe, called the Huygens probe, into the atmosphere of Saturn's moon Titan.

Both missions will be launched by unmanned Titan-4/Centaur-G' boosters, and both are part of the Mariner/Mark-2 series of missions, which will use a new generation of cost-effective modular spacecraft that can easily be modified to accomplish a variety of missions to comets and asteroids and to the outer solar system.

Because of their great distance from the sun, both missions will be powered by RTGs (Radioisotope Thermoelectric Generators). Since the planned schedules do not allow sufficient time for development and flight qualification of new RTG designs, both missions will use generators that are essentially identical to the GPHS-RTGs flown on the recently launched Galileo mission. Two such RTGs will be used for each mission. Their construction will be under the direction of the U.S. Department of Energy's Office of Special Applications (DOE/OSA), which commissioned Fairchild Space Company to conduct RTG studies in support of JPL's design efforts.

The location and orientation of the two RTGs on the spacecraft are functions of numerous, often conflicting, design constraints. The CRAF/Cassini baseline design that JPL asked Fairchild to study is depicted in Figure 1.

Figure 1. CRAF/CASSINI Spacecraft, Baseline Design

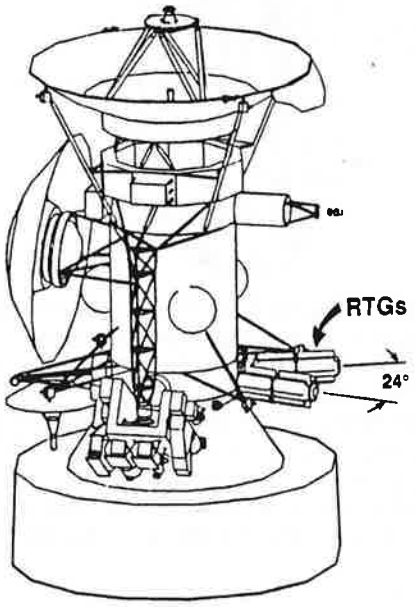

Figure 1 shows the two RTGs cantilevered from the cylindrical spacecraft like radial spokes, with a separation angle of 24 degrees between them. Such proximity leads to mutual obstruction of the two RTGs' heat rejection paths. This obstruction can result in significant axial and circumferential variation of each RTG's cold-junction temperatures and its couples' electrical performance.

To assess the effect of mutual obstructions on the RTGs' output power, Fairchild personnel were asked to analyze the baseline configuration shown in Figure 1, as well as some alternative configurations. Because of the unconventional problem, this required the development of novel analysis methods and computer codes, which are described in this paper. The analytical results reported here will serve as a guide for JPL's spacecraft design decisions.

RTG DESIGN DESCRIPTION

Figure 2 shows a cutaway view of the GPHS-RTG's [2, 3, 4] that will be used on the CRAF and Cassini missions. Each 1.15 m-long RTG contains an axial stack of 18 General Purpose Heat Source modules [5], which radiate their heat to a surrounding cylindrical array of 576 thermoelectric unicouples arranged in 36 layers of 16 couples.

Figure 2. GPHS RTG

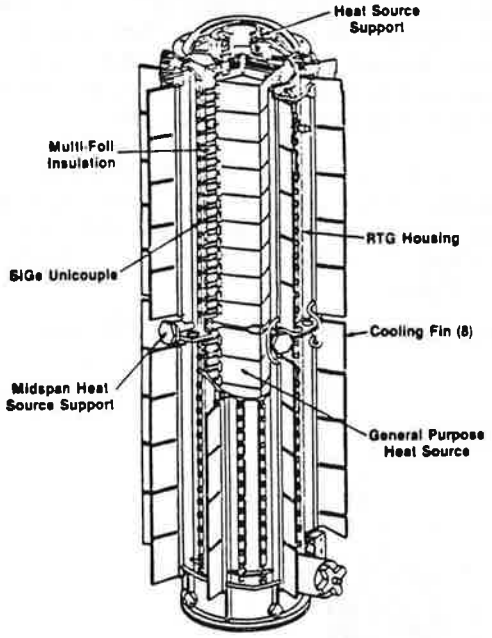

As shown in Figure 3, each unicouple contains a thermoelectric n- and p-leg. These are electrically connected at their hot ends by a hot-shoe, which serves to collect the heat radiated by the centrally located heat source stack and concentrate it at the thermoelectric legs. The cold end of each leg is series- and parallel-connected to adjoining couples to form the RTG's electrical network. The couples' cold ends are bolted to the RTG housing, to which they reject their waste heat. The RTG's waste heat is dissipated by radiation from its housing and its eight equispaced radiator fins, as shown in Figure 2.

Figure 3. Unicouple

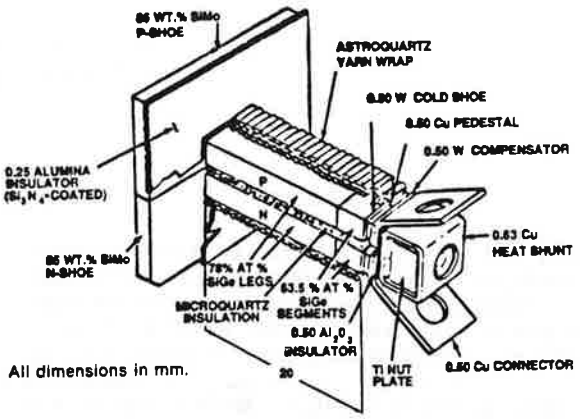

The series-parallel network of the GPHS-RTG is shown in Figure 4, which depicts a rolled-out schematic of the cylindrical array. The electrical network consists of two parallel branches. Each branch contains 144 series-connected groups of two parallel couples. The rather tortuous current path shown is designed to minimize the RTG's self-induced magnetic field.

Figure 4. Current-Path Through GPHS RTG

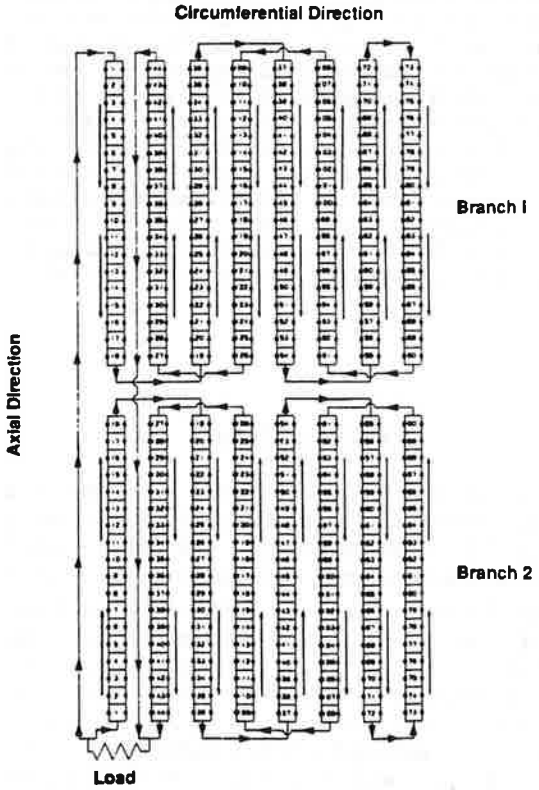

ANALYSIS

The close proximity of the two RTGs on the CRAF/Cassini spacecraft, as illustrated by the baseline design shown in Figure 1, can result in significant mutual blockage of their heat rejection paths. Such blockage would result in circumferential variation of the RTG's housing and cold-junction temperatures. Determining the effect of that temperature variation on the RTGs' power output requires a very detailed and careful analysis, because we are looking for relatively small differences between large numbers, and because even small differences can be quite significant if the mission is power-constrained (as are the CRAF and Cassini missions).

Previous RTG analyses usually made the simplifying assumption that all of the thermoelectric couples in a generator's series-parallel network operate at the same hot- and cold-junction temperatures and at the same current and voltage. For unobstructed RTGs, such a simplified analysis is a useful initial design tool, since it permits closed-form solutions for the optimum area ratio A_n/A_p of the thermoelectric n- and p-legs and for the optimum output voltage. For these optimized parameters, it yields simple expressions for the maximum material efficiency of the thermoelectric couples, and for the required RTG design parameters [6, 7, 8].

But the above simplifying assumptions can introduce significant errors even for unobstructed RTGs, because all RTGs have appreciable axial temperature variations due to unavoidable end losses by radiation and by conduction through the heat source support structure. A more exact analysis, which accounted for the axial temperature variations in a Martian RTG, was reported last year [7, 9]. But that analysis still assumed that the RTG has an axisymmetric view of space and the Martian ground, and therefore no circumferential temperature variation.

The present paper develops a Fairchild-generated methodology and generalized computer code for analyzing the performance of arbitrarily obstructed RTGs with both axial and circumferential temperature, voltage, and current variations, and applies that methodology to the specific example of the CRAF/Cassini baseline design depicted in Figure 1.

COUPLED THERMAL AND ELECTRICAL ANALYSIS

Figure 5 presents the energy balance for a thermoelectric unicouple of leg length **L**, leg areas A_n and A_p, operating between cold- and hot-junction temperatures T_1 and T_2. It gives the couple's thermal conductance **K**, electric resistance **R**, and open-circuit voltage V_o in terms of the temperature-averaged thermal conductivity $\bar{k}$, electrical resistivity $\bar{\rho}$, and Seebeck coefficient $\bar{S}$ of the thermoelectric n- and p-materials. As shown, the heat input rate Q_h at the couple's hot end and the heat rejection rate Q_c at its cold end each consists of four terms: normal heat conduction, Peltier effect, Ohmic dissipation, and Thomson effect. As can be seen, three of those four terms are current-dependent. Therefore, the thermal and electrical analyses cannot be performed separately, but must be conducted simultaneously and interactively.

Figure 5. Unicouple Energy Balance

Open-Circuit Voltage: $V_o = \int (S_n + S_p)\, dT$

Couple Conductance: $K = [\bar{k}_n A_n + \bar{k}_p A_p] / L$

Couple Resistance: $R = [\bar{\rho}_n/A_n + \bar{\rho}_p/A_p] L$

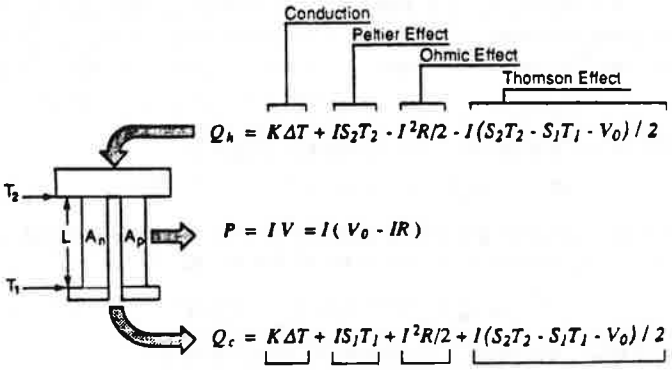

To analyze an RTG of a given design with an unsymmetrically obstructed heat rejection path, a detailed three-dimensional thermal model of the RTG and its environment must be constructed. The hot junction and cold junction of each thermoelectric element in the RTG are represented as discrete nodes. The model cannot be analyzed by means of a standard thermal analysis code, because the connectors between the couple's hot and cold junctions are not simple thermal conductors but include the current-dependent Peltier, Ohmic, and Thomson effects. The rate at which heat enters the connector's hot-end and leaves its cold-end are not equal, since part of the heat entering each couple is converted to electrical energy. That part must in effect be represented as a heat sink for each couple.

The electrical analysis is further complicated by the constraint that each RTG's thermoelectric couples are in general interconnected in a complex series-parallel network, and that all couples grouped in parallel must operate at the same output voltage, and that all couple groups in series must produce the same current.

The RTG analysis methodology developed by Fairchild is generic, not just for the GPHS-RTG network shown in Figure 4. In general, the equivalent

circuit of an RTG network consists of **B** parallel branches, with each branch containing **G** series-connected groups of **C** parallel couples. Each thermoelectric element in the RTG is designated by a branch number **b**, group number **g**, and couple number **c**, where:

$$1 \le b \le B,$$
$$1 \le g \le G,$$
$$1 \le c \le C.$$

For the case of the GPHS-RTG, **B=2**, **G=144**, **C=2**, and the equivalent circuit of the generator is shown in Figure 6.

Figure 6. Equivalent Circuit of GPHS RTG

ELECTRICAL ANALYSIS

For each couple in the RTG, the difference between its open-circuit voltage $V_O(b,g,c)$ and its internal voltage drop $I(b,g,c)\,R(b,g,c)$ equals its output voltage $V(b,g,c)$. Since the couples in each group **b,g** are connected in parallel, their output voltage must equal the group voltage $V(b,g)$.

$$V_O(b,g,c) - I(b,g,c)\,R(b,g,c) = V(b,g,c) = V(b,g)$$

Therefore, the current through couple **b,g,c** is:

$$I(b,g,c) = \left[\, V_O(b,g,c) - V(b,g) \,\right] / R(b,g,c)\,.$$

The sum of each group's **C** couple currents equals the group current **I(b,g)**. Since all groups in each branch **b** are connected in series, this must equal the branch current **I(b)**:

$$\sum_{c=1}^{C} \left[\, V_O(b,g,c) / R(b,g,c) \,\right] - V(b,g) \sum_{c=1}^{C} \left[1/R(b,g,c) \right] = I(b,g) = I(b)$$

Therefore, the voltage produced by group **b,g**, is:

$$V(b,g) = \left\{ \sum_{c=1}^{C} \left[\, V_O(b,g,c) / R(b,g,c) \,\right] - I(b) \right\} / \sum_{c=1}^{C} \left[1/R(b,g,c) \right]$$

The sum of the **G** group voltages in each branch equals the branch voltage **V(b)**. Since the **B** branches are connected in parallel, this also equals the RTG's output voltage V_{RTG}:

$$\sum_{g=1}^{G} \left\{ \sum_{c=1}^{C} \left[\, V_O(b,g,c) / R(b,g,c) \,\right] / \sum_{c=1}^{C} \left[1/R(b,g,c) \right] \right\} - I(b) \sum_{g=1}^{G} \left\{ 1/\sum_{c=1}^{C} \left[1/R(b,g,c) \right] \right\} = V(b) = V_{RTG}\,.$$

Solving for the branch current **I(b)** for each branch and summing the currents for the **B** parallel branches gives the RTG output current:

$$I_{RTG} = \sum_{b=1}^{B} \left\{ \left[\sum_{g=1}^{G} \left\{ \sum_{c=1}^{C} \left[\, V_O(b,g,c) / R(b,g,c) \,\right] / \sum_{c=1}^{C} \left[1/R(b,g,c) \right] \right\} - V_{RTG} \right] / \sum_{g=1}^{G} \left\{ 1/\sum_{c=1}^{C} \left[1/R(b,g,c) \right] \right\} \right\}.$$

The above equation represents the current-voltage characteristic of the RTG network. It can be expressed in the condensed form

$$I_{RTG} = I_{SC} - V_{RTG}/R_{RTG}\,,$$

where I_{SC} is the RTG's short-circuit current, defined by

$$I_{SC} = \sum_{b=1}^{B} \left[\sum_{g=1}^{G} \left\{ \sum_{c=1}^{C} \left[\, V_O(b,g,c) / R(b,g,c) \,\right] / \sum_{c=1}^{C} \left[1/R(b,g,c) \right] \right\} / \sum_{g=1}^{G} \left\{ 1/\sum_{c=1}^{C} \left[1/R(b,g,c) \right] \right\} \right],$$

and R_{RTG} is the RTG's internal resistance, defined by

$$R_{RTG} = 1/\sum_{b=1}^{B} \left[1/\sum_{g=1}^{G} \left\{ 1/\sum_{c=1}^{C} \left[1/R(b,g,c) \right] \right\} \right]\,.$$

ITERATIVE COMPUTATIONS

For each iteration in the analysis, the code uses each couple's cold- and hot-junction temperatures T_1 and T_2 (from the preceding iteration) to compute its temperature-averaged properties $\bar{k}$ and $\bar{\rho}$, open-circuit voltage V_o, thermal conductance K and electrical resistance R:

$$\bar{k}_n(b,g,c) = \int_{T_1(b,g,c)}^{T_2(b,g,c)} k_n(T)\, dT \,/\, [\, T_2(b,g,c) - T_1(b,g,c)\,]$$

$$\bar{k}_p(b,g,c) = \int_{T_1(b,g,c)}^{T_2(b,g,c)} k_p(T)\, dT \,/\, [\, T_2(b,g,c) - T_1(b,g,c)\,]$$

$$\bar{\rho}_n(b,g,c) = \int_{T_1(b,g,c)}^{T_2(b,g,c)} \rho_n(T)\, k_n(T)\, dT \,/\, \bar{k}_n(b,g,c)\,[\, T_2(b,g,c) - T_1(b,g,c)\,]$$

$$\bar{\rho}_p(b,g,c) = \int_{T_1(b,g,c)}^{T_2(b,g,c)} \rho_p(T)\, k_p(T)\, dT \,/\, \bar{k}_p(b,g,c)\,[\, T_2(b,g,c) - T_1(b,g,c)\,]$$

$$V_O(b,g,c) = \int_{T_1(b,g,c)}^{T_2(b,g,c)} [\, S_n(T) + S_p(T)\,]\, dT$$

$$K(b,g,c) = [\, \bar{k}_n(b,g,c)\, A_n + \bar{k}_p(b,g,c)\, A_p \,] \,/\, L$$

$$R(b,g,c) = [\, \bar{\rho}_n(b,g,c) \,/\, A_n + \bar{\rho}_p(b,g,c) \,/\, A_p \,]\, L$$

Using these values of V_O, K, and R for each couple and the prescribed RTG voltage V_{RTG}, the code computes the branch current I(b) for each of the B branches,

$$I(b) = \Big[\sum_{g=1}^{G} \Big\{ \sum_{c=1}^{C} [\, V_O(b,g,c) / R(b,g,c)\,] \Big/ \sum_{c=1}^{C} [\, 1/R(b,g,c)\,] \Big\} - V_{RTG} \Big] \Big/ \sum_{g=1}^{G} \Big\{ 1/\sum_{c=1}^{C} [\, 1/R(b,g,c)\,] \Big\} ,$$

the group voltage V(b,g) for each of the G groups in each branch,

$$V(b,g) = \Big\{ \sum_{c=1}^{C} [\, V_O(b,g,c) / R(b,g,c)\,] - I(b) \Big\} \Big/ \sum_{c=1}^{C} [\, 1/R(b,g,c)\,] ,$$

and the couple current I(b,g,c) for each couple in the RTG,

$$I(b,g,c) = [\, V_O(b,g,c) - V(b,g)\,] \,/\, R(b,g,c).$$

The individual couple currents are then used to compute the hot-end heat input rate Q_H(b,g,c,) and the cold-end heat rejection rate Q_C(b,g,c) for each couple:

$$Q_H(b,g,c) = K(b,g,c)\,[\, T_2(b,g,c) - T_1(b,g,c)\,] - I^2(b,g,c)\, R(b,g,c) \,/\, 2 + I(b,g,c)\,[\, S_2(b,g,c)\, T_2(b,g,c) + S_1(b,g,c)\, T_1(b,g,c) + V_O(b,g,c)\,] \,/\, 2 ,$$

$$Q_C(b,g,c) = K(b,g,c)\,[\, T_2(b,g,c) - T_1(b,g,c)\,] + I^2(b,g,c)\, R(b,g,c) \,/\, 2 + I(b,g,c)\,[\, S_2(b,g,c)\, T_2(b,g,c) + S_1(b,g,c)\, T_1(b,g,c) - V_O(b,g,c)\,] \,/\, 2 ,$$

where S_1 and S_2 denote the Seebeck coefficients at the cold- and hot-junction of the couple.

The code inserts these heat flow rates for each couple in the RTG into the detailed thermal analysis model for the next iteration; and repeats the procedure until convergence is achieved.

CODE VALIDATION

The code was first tested in the analyses of an unobstructed generator, with axial temperature variation but no circumferential variation. It was validated by using it to analyze the performance of the electrically heated thermoelectric generator (ETG) that had been employed as the engineering test unit [10], a prototype of the GPHS-RTGs used for the Galileo mission. The reason for using the ETG instead of the RTG as a validation check for the code is that the ETG test measurements include the thermocouples' hot-shoe temperatures, but - because of practical difficulties - the RTG measurements do not.

The analysis of the ETG's performance was based on thermoelectric properties of SiGe aged for one year to account for pre-test outgassing and processing. The temperature-dependent values of resistivity, conductivity, and Seebeck coefficient of the n- and p-material used in the analysis are summarized in Table 1.

Table 1. Thermoelectric Properties Model

Temp °C	Seebeck μV/K		Resistivity mΩ.cm		Conductivity mW/cm.K	
	N	P	N	P	N	P
0	90	114	0.79	0.91	51.4	58.4
50	113	128	0.87	0.95	50.2	57.2
100	135	140	0.95	1.01	49.0	56.3
150	153	152	1.04	1.08	47.9	55.0
200	168	163	1.13	1.15	46.8	54.1
250	185	173	1.28	1.24	45.8	52.9
300	215	183	1.72	1.32	44.7	51.7
350	265	192	2.77	1.42	43.9	51.0
400	304	202	3.81	1.53	43.1	49.9
450	317	211	4.17	1.64	42.5	49.1
500	317	220	4.02	1.74	41.8	48.2
550	312	229	3.75	1.87	41.5	47.5
600	306	240	3.46	2.06	41.0	46.8
650	298	256	3.13	2.38	40.8	46.2
700	289	287	2.82	2.98	40.6	45.7
750	280	320	2.53	4.49	40.6	45.3
800	273	331	2.28	4.76	40.7	45.2
850	268	330	2.09	4.54	40.9	45.4
900	264	323	1.95	4.17	41.4	46.0
950	263	318	1.86	3.84	42.1	47.1
1000	263	316	1.82	3.57	43.4	49.2
1050	262	314	1.77	3.22	45.6	52.2
1075	262	314	1.75	3.10	46.9	54.3

The analytical results were compared with the ETG test measurements. For the same RTG thermal power and the same average cold-junction temperature, the experimental measurements and the analytical results produced by the code were in very good agreement. The average hot-junction temperatures agreed within 5°C (986 versus 981), and the electrical power outputs agreed within 1 watt (296 versus 297).

As a further check on the validity of the analytical model, it was used to compute the BOM performance of one of the Galileo flight RTGs (F4). For the same thermal power, it yielded an electrical output of 285.6 watts, compared to the measured output power of 287.7 watts in Earth orbit. This agreement is better than the estimated 1.2% telemetry error.

The good agreement between the analytical and experimental results for both the ETG and the RTG lends confidence to our use of the same model and assumptions for subsequent analyses of the initial RTG output at various thermal powers and external environments.

ANALYSIS OF OBSTRUCTED CRAF/CASSINI RTGs

The application of the code to the analysis of the obstructed CRAF/Cassini RTGs started with the construction of a 1912-node radiation-interchange analysis model. The model represented the housing and fins of the GPHS-RTG pictured in Figure 2 and the spacecraft shown in Figure 1. The ITAS (Integrated Thermal Analysis System) code [11], which accounts for the effect of mutual reflections, was used to compute over 102,000 radiation interchange factors between all surface nodes that are within each other's view. The computed radiation interchange factors were then inserted into a detailed thermal and electrical analysis model consisting of ~2900 node points.

The coupled thermal and electrical analysis was carried out by means of the previously discussed computer code. The code was based on the SINDA thermal analysis program [12], modified by us to incorporate the current-dependent Peltier, Ohmic, and Thomson effects on thermocouple conductance and to represent the electrical power generation in each couple as an effective heat sink. In each iteration, the modified code computed each couple's heat input rate and heat rejection rate and inserted them into the thermal analysis for the next iteration. After the solution had homed in to prescribed convergence criteria, it was used to calculate the RTG's electrical output and efficiency.

To illustrate typical results, the converged BOM solution for the baseline configuration and a thermal power of 245 watts from each of the 18 heat source modules is summarized in Tables 2 through 5. The tables display the results for the flattened-out cylindrical array of 576 thermocouples in the RTG.

Table 2 shows the axial and circumferential variation of the RTG's cold-junction temperatures. As can be seen these vary from 276°C for the least obstructed couple to 302°C for the most obstructed couple. The last column and last line of the table show the variation of the averaged cold-junction temperatures in the axial and circumferential directions, respectively. As shown, the average temperature is lowest near the ends of the RTG, and highest near the RTG's midplane. Circumferentially, the average temperature is lowest in Column 6, the outward-facing side of the RTG, and highest in Column 14, the RTG side facing the neighboring RTG.

Table 3 similarly shows the axial and circumferential variations of the baseline RTG's hot-junction temperatures. As can be seen, the couples' average hot-junction temperatures vary by 35°C in the axial direction, and show almost no variation in the circumferential direction. Thus, the obstruction by the neighboring RTG and by the spacecraft affects only the cold-junction temperatures, and produces only a negligible circumferential variation of the hot-junction temperatures. In addition to the hot-junction temperatures, the table shows the axial variation of the heat source surface temperatures. As shown by the table's left column, these vary from 1008°C at the upper outboard end of the heat source stack to 1042°C near the middle of the stack.

The consequent variation in the thermocouples' temperature-spans affects their electrical performance. The axial and circumferential variations of the couple voltages is displayed in Table 4, and those of the couple currents in Table 5. The sixteen columns in these tables represent eight column pairs of parallel couples. Table 4 shows that all parallel couples have the same output voltage, ranging from 0.197 volt to 0.215 volt; and Table 5 shows that all couple pairs in each branch have the same combined output current, as demanded by the RTG's series-parallel network.

As can be seen, the network's two branches have respective output currents 5.14 and 5.16 amp, for a total output of 10.30 amps per RTG. The 144 series-connected couple groups in each branch produce 30.0 volts. Subtracting 0.34 volts for ohmic losses in the RTG's series leads leaves a net output of 29.66 volts and 309 watts per RTG. The average material efficiency of the couples is 7.90%; the average couple efficiency (including the effect of contact resistances and electrode losses) is 7.55%; and the net system efficiency (including the effect of heat losses through the thermal insulation and through the heat source support structure) is 7.01%.

Table 2. Cold-Junction Temperatures (°C)

	1	2	3	4	5	6	7	8	9	10	11	12	13	14	15	16	AVG.
2	280	279	277	277	276	276	276	277	277	278	279	280	282	282	282	282	279
4	282	281	279	279	278	278	278	279	279	280	281	283	284	285	285	284	281
6	285	283	282	281	280	280	280	281	281	282	283	285	287	288	287	287	283
8	287	285	284	283	282	282	282	283	283	284	286	287	290	290	290	289	285
10	289	287	285	284	284	284	284	284	285	286	287	290	292	293	292	292	287
12	291	289	287	286	285	285	285	285	286	287	289	291	294	295	295	294	289
14	293	290	288	287	286	286	286	287	288	290	293	296	297	296	295	296	290
16	294	291	289	288	287	286	287	287	288	289	291	294	297	298	298	297	291
18	295	292	290	288	287	287	287	287	288	290	292	295	298	299	299	298	292
20	296	293	290	289	288	287	287	288	289	290	293	296	299	300	300	299	293
22	296	293	291	289	288	287	287	288	289	290	293	296	300	301	301	300	293
24	297	293	291	289	288	287	287	287	289	290	293	296	300	301	302	300	293
26	296	293	290	288	287	287	286	287	288	290	293	296	300	301	302	300	293
28	296	292	289	288	286	286	286	286	287	289	292	296	300	301	301	300	292
30	295	291	288	286	285	284	284	285	286	288	291	295	299	300	300	299	291
32	293	289	287	285	283	283	283	283	285	286	289	293	297	298	298	297	289
34	291	287	285	283	282	281	281	282	283	285	287	291	295	296	296	295	288
36	289	285	283	281	280	279	279	280	281	283	285	289	293	294	294	292	285
AVG.	291	289	286	285	284	284	284	284	285	286	289	291	295	296	295	294	289

Table 3. Hot-Junction Temperatures (°C)

R.S.		1	2	3	4	5	6	7	8	9	10	11	12	13	14	15	16	AVG.
1008	2	975	975	975	975	975	975	975	975	975	975	975	975	975	975	975	975	975
1017	4	984	984	984	983	983	983	983	983	984	984	984	984	984	984	984	984	984
1023	6	991	991	991	990	990	990	990	990	991	991	991	991	991	991	991	991	991
1029	8	996	996	996	996	996	996	996	996	996	996	996	996	996	996	996	996	996
1033	10	1001	1001	1000	1000	1000	1000	1000	1000	1000	1000	1001	1001	1001	1001	1001	1001	1001
1036	12	1004	1004	1004	1004	1004	1004	1004	1004	1004	1004	1004	1004	1004	1004	1004	1004	1004
1038	14	1007	1006	1006	1006	1006	1006	1006	1006	1006	1006	1006	1006	1007	1007	1007	1007	1006
1040	16	1008	1008	1008	1008	1008	1008	1008	1008	1008	1008	1008	1008	1009	1009	1009	1009	1008
1041	18	1010	1009	1009	1009	1009	1009	1009	1009	1009	1009	1009	1010	1010	1010	1010	1010	1009
1042	20	1010	1010	1010	1010	1010	1010	1010	1010	1010	1010	1010	1010	1010	1010	1010	1010	1010
1042	22	1010	1010	1010	1010	1010	1010	1010	1010	1010	1010	1010	1010	1010	1010	1010	1010	1010
1041	24	1009	1009	1009	1009	1009	1009	1009	1009	1009	1009	1009	1009	1009	1009	1009	1009	1009
1039	26	1008	1007	1007	1007	1007	1007	1007	1007	1007	1007	1007	1007	1008	1008	1008	1008	1007
1037	28	1005	1005	1005	1005	1005	1005	1005	1005	1005	1005	1005	1005	1005	1005	1006	1005	1005
1034	30	1002	1002	1002	1002	1002	1002	1002	1002	1002	1002	1002	1002	1002	1002	1002	1002	1002
1030	32	998	998	998	998	997	997	997	997	997	998	998	998	998	998	998	998	998
1025	34	992	992	992	992	992	992	992	992	992	992	992	992	992	992	992	992	992
1018	36	985	985	985	985	985	985	985	985	985	985	985	985	985	985	985	985	985
	AVG.	1000	1000	1000	999	999	999	999	999	999	1000	1000	1000	1000	1000	1000	1000	1000

Table 4. Couple Voltage (mV)

	1	2	3	4	5	6	7	8	9	10	11	12	13	14	15	16	AVG.
2	199	199	200	200	201	201	201	201	200	200	199	199	198	198	198	198	199
4	203	203	204	204	205	205	205	205	204	204	203	203	201	201	202	202	203
6	206	206	207	207	208	208	208	208	207	207	206	206	204	204	204	204	206
8	208	208	210	210	210	210	210	210	209	209	208	208	206	206	206	206	208
10	210	210	211	211	212	212	212	212	211	211	209	209	207	207	207	207	210
12	211	211	212	212	213	213	213	213	212	212	210	210	208	208	208	208	211
14	211	211	213	213	214	214	214	214	213	213	211	211	209	209	209	209	212
16	212	212	214	214	215	215	215	215	214	214	212	212	209	209	209	209	212
18	212	212	214	214	215	215	215	215	214	214	212	212	209	209	209	209	213
20	211	211	214	214	215	215	215	215	214	214	211	211	208	208	208	208	212
22	211	211	214	214	215	215	215	215	214	214	211	211	208	208	208	208	212
24	210	210	213	213	214	214	214	214	213	213	210	210	207	207	207	207	211
26	210	210	212	212	214	214	214	214	213	213	210	210	206	206	206	206	210
28	209	209	211	211	213	213	213	213	212	212	209	209	205	205	205	205	209
30	207	207	210	210	212	212	212	212	210	210	207	207	204	204	204	204	208
32	206	206	208	208	210	210	210	210	209	209	206	206	202	202	202	202	206
34	203	203	206	206	208	208	208	208	206	206	203	203	200	200	200	200	204
36	200	200	203	203	204	204	204	204	203	203	200	200	197	197	197	197	201
AVG.	208	208	210	210	211	211	211	211	210	210	208	208	205	205	205	205	208

Table 5. Couple Current (amp)

	1	2	3	4	5	6	7	8	9	10	11	12	13	14	15	16	AVG.
2	2.57	2.58	2.58	2.57	2.57	2.57	2.57	2.57	2.58	2.57	2.57	2.58	2.57	2.57	2.57	2.57	2.57
4	2.57	2.58	2.58	2.57	2.57	2.57	2.57	2.57	2.58	2.57	2.57	2.58	2.57	2.57	2.57	2.57	2.57
6	2.57	2.58	2.58	2.57	2.57	2.57	2.57	2.57	2.58	2.57	2.57	2.58	2.57	2.57	2.57	2.57	2.57
8	2.57	2.58	2.58	2.57	2.57	2.57	2.57	2.57	2.58	2.57	2.57	2.58	2.57	2.57	2.57	2.58	2.57
10	2.56	2.58	2.58	2.57	2.57	2.57	2.57	2.57	2.58	2.57	2.56	2.58	2.57	2.57	2.57	2.58	2.57
12	2.56	2.58	2.58	2.57	2.57	2.57	2.57	2.57	2.58	2.57	2.56	2.58	2.57	2.57	2.57	2.58	2.57
14	2.56	2.58	2.58	2.57	2.57	2.57	2.57	2.57	2.58	2.57	2.56	2.58	2.57	2.58	2.57	2.58	2.57
16	2.56	2.58	2.58	2.57	2.57	2.57	2.57	2.57	2.58	2.57	2.56	2.58	2.57	2.58	2.57	2.58	2.57
18	2.56	2.58	2.58	2.57	2.57	2.57	2.57	2.57	2.58	2.57	2.56	2.58	2.57	2.58	2.57	2.58	2.57
20	2.57	2.59	2.59	2.57	2.58	2.58	2.58	2.58	2.59	2.57	2.57	2.59	2.58	2.58	2.58	2.58	2.58
22	2.57	2.59	2.59	2.57	2.58	2.58	2.58	2.58	2.59	2.57	2.57	2.59	2.58	2.58	2.58	2.58	2.58
24	2.57	2.59	2.59	2.57	2.58	2.58	2.58	2.58	2.59	2.57	2.57	2.59	2.58	2.58	2.58	2.58	2.58
26	2.57	2.59	2.59	2.57	2.58	2.58	2.58	2.58	2.59	2.57	2.57	2.59	2.58	2.58	2.58	2.58	2.58
28	2.57	2.59	2.59	2.57	2.58	2.58	2.58	2.58	2.59	2.57	2.57	2.59	2.58	2.58	2.58	2.58	2.58
30	2.57	2.59	2.59	2.57	2.58	2.58	2.58	2.58	2.59	2.57	2.57	2.59	2.58	2.58	2.58	2.58	2.58
32	2.57	2.59	2.59	2.57	2.58	2.58	2.58	2.58	2.59	2.57	2.57	2.59	2.58	2.58	2.58	2.58	2.58
34	2.57	2.59	2.59	2.57	2.58	2.58	2.58	2.58	2.59	2.57	2.57	2.59	2.58	2.58	2.58	2.58	2.58
36	2.57	2.59	2.59	2.57	2.58	2.58	2.58	2.58	2.59	2.57	2.57	2.59	2.58	2.58	2.58	2.58	2.58
AVG.	2.57	2.59	2.58	2.57	2.58	2.57	2.58	2.57	2.58	2.57	2.57	2.59	2.57	2.58	2.57	2.58	2.58

The 7-watt performance penalty at a 24-degree separation does not seem large. But both missions are severely power-constrained, and the JPL designers are reluctant to give up 14 watts from the two RTGs. Design modifications for reducing or even eliminating that performance penalty are possible and should be investigated.

Equally detailed coupled thermal and electrical analyses were performed for thermal power levels ranging from 225 to 250 watts per heat source module, for both obstructed and unobstructed RTGs. The unobstructed units had axial temperature variations but no circumferential variation. The principal results for the mutually obstructed RTGs in the CRAF/Cassini baseline configuration (Figure 1) and the comparative results for an unobstructed RTG are displayed in Figures 7, 8, and 9.

Figures 7 and 8 respectively show the effect of the thermal power Q per heat source module on the RTG power output and on the average hot-junction temperature. As can be seen, both relationships are essentially linear, and the figures present least-square curve fits for the respective curves. These curve fits are useful design tools, and will be used in predicting the effect of fuel decay on RTG power and temperature.

Figure 7. Effect of Thermal Power on BOM Electrical Power

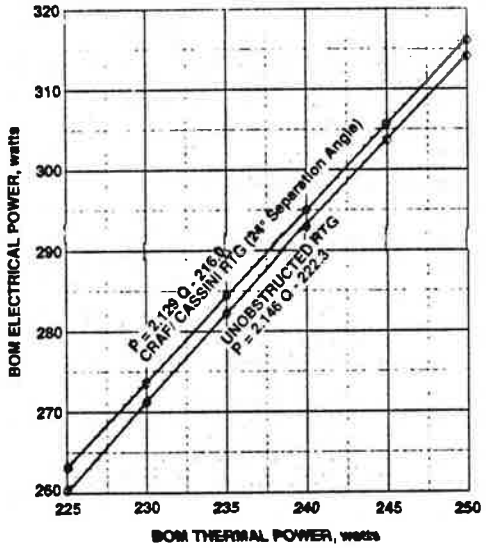

The two figures show that, for a given thermal power, the obstruction by the neighboring RTG has very little effect on the RTG's power output, but has a significant effect on its hot-junction temperature, which affects the degradation rate. Figure 9 presents cross-plots showing the relationship between maximum hot-junction temperatures and BOM power outputs for unobstructed RTGs and for *mutually* obstructed RTGs with a 24-degree separation angle.

The performance of the obstructed and unobstructed RTGs should be compared for the same maximum hot-junction temperature, since that is what limits the RTG's degradation rate and lifetime. Previous SiGe flight units (LES 8/9, Voyager, Galileo) were designed for a maximum hot-junction temperature of 1000°C. For that temperature, Figure

Figure 8. Effect of Thermal Power on Average Hot-Junction Temperature

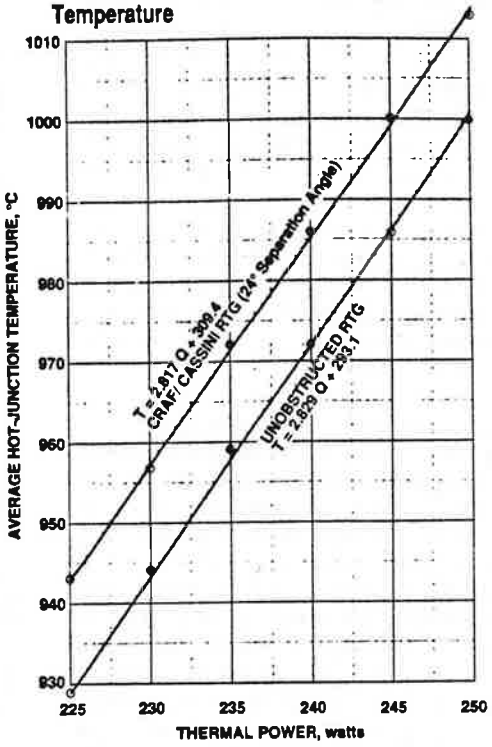

Figure 9. Effect of Obstruction By Neighboring RTG on Power-Versus-Temperature Characteristics

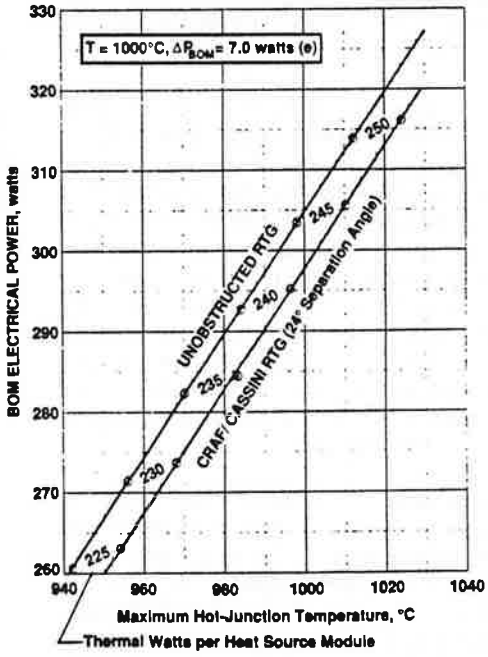

9 shows that the CRAF/Cassini RTG's power output is reduced by 7.0 watts (2.5%) for the 24-degree separation angle of the baseline configuration. Similar analyses showed a reduction of 13 watts (4.3%) for a 16-degree separation angle. This demonstrates the sensitivity of power output to separation angle.

LONG-TERM PERFORMANCE DEGRADATION

In addition to BOM power, the system designer is of course interested in the RTGs' EOM power. The principal factors that diminish an RTG's power output with time are fuel decay and thermoelectric degradation. The thermal power Q at mission time t is given by

$$Q/Q_1 = 0.5^{t/\tau},$$

where Q_1 is the thermal power at the beginning of the mission and τ is the isotope's half-life (87 years). The corresponding undegraded electrical power P_u is given by

$$P_u = a_p + b_p Q_1 (0.5)^{t/\tau},$$

where a_p and b_p are curve-fit coefficients obtained from Figure 7.

Predicting the thermoelectric performance degradation with time is generally a complex problem, since many different degradation mechanisms are at play. A detailed method for making such predictions is the DEGRA code developed by V. Raag in the early 70's [13], but that code does not account for the detailed effects of mutual obstruction between neighboring RTGs. In the same time period, A. Mowery [14] performed statistical analyses of test results which showed that the degradation of electrically heated thermoelectric converters employing SiGe unicouples at constant temperatures can be quite accurately predicted by the simple empirical equation

$$P/P_1 = 1 - \alpha\sqrt{t},$$

where α is a proportionality factor whose dependence on the hot junction's absolute temperature T is given by the Arrhenius function

$$\alpha = a_\alpha \exp(-b_\alpha/T),$$

where $a_\alpha = 6973\ yr^{-1/2}$ and $b_\alpha = 15{,}480°K$

These empirical expressions were found to give excellent agreement with the experimental data from the electrically heated tests at various constant thermal powers and temperatures. However, Mowery's equations cannot be directly applied to predict the performance degradation of RTGs because an RTG operates at a given fuel loading at a diminishing thermal power and temperature, and therefore at diminishing degradation rates. What is needed is an equation that corrects for the diminishing value of α as the temperature decreases with time . To account for that effect, the present author developed the following simple modification of Mowery's original equation:

$$P/P_1 = 1 - \left[\int_0^t \alpha^2 dt\right]^{1/2}.$$

This modification appears quite plausible, but its validity must be confirmed by comparing its results to long-term tests with variable Q and T. (Note that for the special case of constant T and therefore constant α, the modified equation reduces to Mowery's validated equation.)

To apply the above equations, we require an expression for hot-junction temperature T as a function of mission time t:

$$T = a_T + b_T Q_1 (0.5)^{t/\tau},$$

where a_T and b_T are the curve-fit coefficients obtained from Figure 8, but with a_T adjusted to express T in Kelvin.

The above equations can be combined to yield an expression giving the combined effect of fuel decay and thermoelectric degradation on the RTG's output power P as a function of mission time t:

$$P = (a_p + b_p Q_1 (0.5)^{t/\tau})\left\{1 - a_\alpha\left[\int_0^t \exp\left(-\frac{2b_\alpha}{a_T + b_T Q_1 (0.5)^{t'/\tau}}\right)dt'\right]^{1/2}\right\}$$

VALIDATION OF DEGRADATION MODEL

The above equations were applied to the Q-1 RTG, which was the qualification unit for the GPHS-RTGs used on the Galileo mission. The computed results are shown in Figure 10. The curve labeled Q/Q_1 shows the thermal power decay, and the curve labeled T shows the resultant decrease in average hot-junction temperature. The curve labeled P_u/P_1 shows the power loss due to fuel decay for undegraded thermoelectric performance, and the curve labeled P/P_u shows the power loss due to thermoelectric degradation. The combined effect of fuel decay and thermoelectric degradation is shown by the curve labeled P/P_1. As can be seen, the combined effect is predicted to result in a 23.6% power loss in 12 years.

Figure 10. Effect of Fuel Decay and Thermoelectric Degradation on Performance of Galileo Qualification RTG (Q-1)

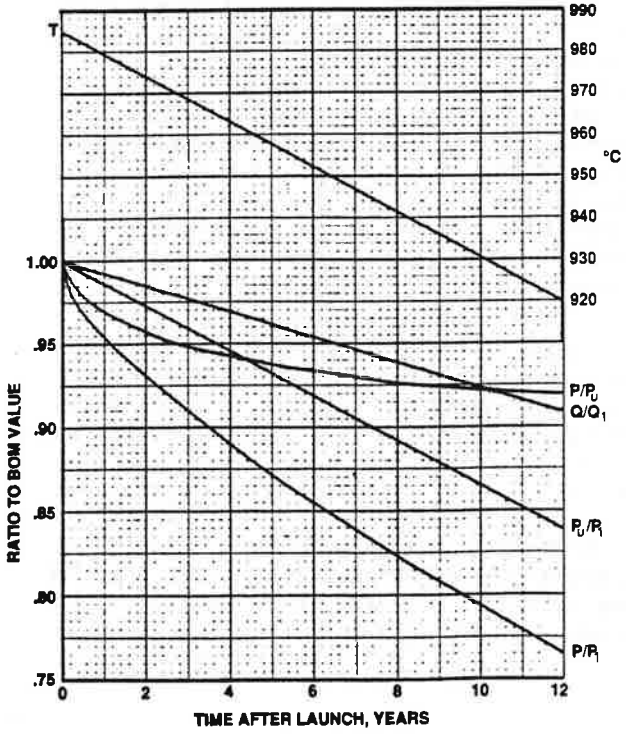

Figure 11 shows a comparison of these predictions with the measured results of a five-year test of the Q-1 RTG. As can be seen, for the range of times and temperatures tested, the rather simple prediction model used showed surprisingly good agreement with the experimental results.

Figure 11. Comparison of Predicted and Measured Power History of Q-1 RTG

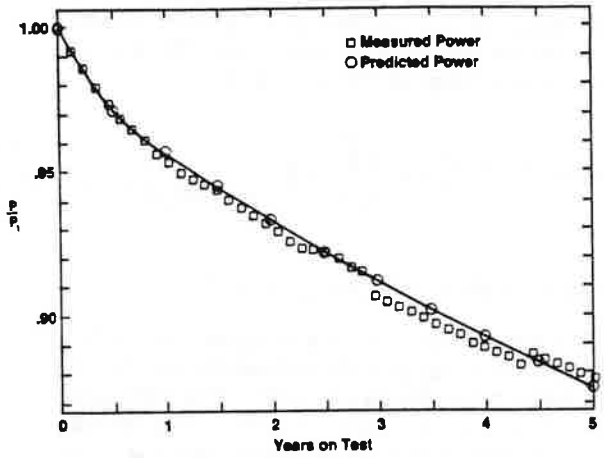

APPLICATION TO CRAF AND CASSINI RTGs

Finally, the analytical methodology described above was used to predict the long-term power degradation of the spacecraft-integrated CRAF and Cassini RTGs, positioned as depicted in the baseline design of Figure 1. The analytical results are shown in Figure 12. For various initial thermal power levels, the figure shows the variation of RTG power and average hot-junction temperature with time. Thus, the figure can be employed as a useful design tool by the CRAF and Cassini mission planners.

Figure 12 shows that increasing the BOM thermal power (by increasing the fuel loading) leads to a substantial increase of the RTG's electrical power at the beginning of mission, but that this benefit diminishes towards the end of mission, particularly for long mission times. This comes about because higher thermal powers result in higher temperatures and therefore higher degradation rates. In fact, at unrealistically high hot-junction temperatures (>1100°C) increasing the thermal power can actually decrease the EOM electrical power.

Figure 12 can be used directly to predict the power history of the two RTGs for the Cassini mission, since those will both be new units. However, for the CRAF mission only one RTG will be new, and the other will be a left-over spare unit from the Galileo program. The fuel of that unit was encapsulated in 1982, and will have decayed for 13 years by the time the CRAF spacecraft's scheduled launch in 1995. As a result, by the beginning of the mission its thermal power will have dropped from 252 watts to 227 watts per heat source module.

Figure 12. Effect of Fuel Loading on Power and Temperature History of CRAF/CASSINI RTGs

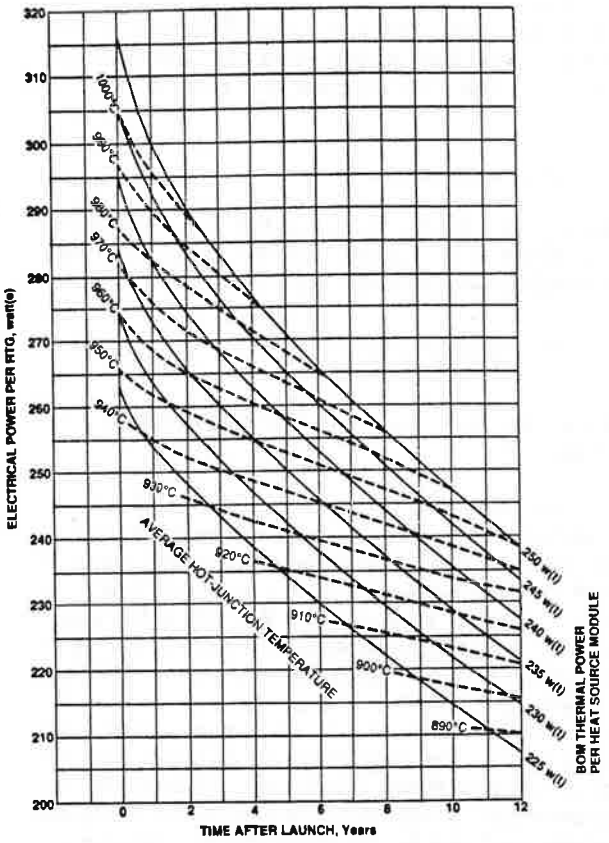

During almost all of the 13-year storage interval, the old RTG will have been filled with an inert cover gas, to spoil its multifoil thermal insulation, lower its hot-junction temperature, and virtually eliminate its thermoelectric degradation. Thus, the spacecraft will be launched with two RTGs having similar thermoelectric properties but substantially different thermal powers and temperatures. To determine the effect of the two unequal RTGs on each other, a detailed BOM thermal and electrical analysis of the baseline-configured RTGs with respective thermal powers of 245 and 227 watts per heat source module was carried out. The results fell right on the curves shown in Figures 7 and 8 for obstructed but equal RTGs. In other words, each RTG is affected by the obstruction of its neighbor, but its resultant power loss is essentially independent of its neighbor's thermal power. Therefore, Figure 12 can also be used to predict the performance history of the two unequal RTGs on the CRAF mission, by using appropriate BOM thermal powers.

RESULTS AND CONCLUSIONS

If JPL were ready to issue power requirement profiles for the CRAF and Cassini missions, these could be superimposed on Figure 12 to identify what BOM thermal power the new RTGs must have to

satisfy those missions. JPL has not yet issued such requirement profiles, but they have specified specific power requirements at two critical times in each of the two missions [15]. These are shown at the top of Table 6. We can therefore use Figure 12 to determine whether the maximum available fuel loadings are sufficient to satisfy the power requirements at those four points in the missions. This determination is summarized in the rest of the table.

Table 6. Power Margins in CRAF/CASSINI RTGs

MISSION	CRAF		CASSINI	
Event	Rendezvous	Perihelion	Arrival	EOM
Years After Launch	5.01	7.61	6.50	10.30
Mission Power Requirement (watts)	458	432	524	478
RTG #	1 2	1 2	1 2	1 2
Age of Fuel at Launch (years)	3 13	3 13	3 3	3 3
Thermal Power per H.S. Module (watts)				
At Fuel Encapsulation	252 252	252 252	252 252	252 252
At Launch (BOM)	245 227	245 227	245 245	245 245
Hot-Junction Temperature (°C)				
At Launch	1000 952	1000 952	1000 1000	1000 1000
At Event	973 924	960 910	966 966	946 946
Electrical Power (watts)				
At Launch	305 267	305 267	305 305	305 305
At Event	265 237	253 226	258 258	241 241
Total at Event	502	479	516	482
Power Margin (watts)	44	47	−8	−4

The General Purpose Heat Source modules [5] have a nominal thermal power of 250 watts at the time of fuel encapsulation. Specifically,their power is a function of achievable fuel density and enrichment. In fact, a typical Galileo flight generator (F1) had an actual beginning-of-life thermal power of 252 watts per heat source module. Assuming a three-year interval between fuel encapsulation and launch, this would yield a BOM thermal power of 245 watts per module for the three new RTGs. The resultant hot-junction temperatures and power outputs of each RTG at launch and at the time of the four JPL-specified events were obtained from Figure 12 and are listed in Table 6. For each event, the predicted power output of the two RTGs is summed, and compared to JPL's specified power requirement to determine the available power margin.

As shown in Table 6, at the 24-degree separation angle of JPL's baseline design, the mutually obstructed standard GPHS/RTGs (with the same fuel loading as was used in the Galileo mission) show adequate power margins for the CRAF mission, but slightly negative margins for the Cassini mission. These Cassini power margins could be raised to acceptable levels by modifying either the payload power demand, or the RTG location on the spacecraft, or the RTG design (if the program schedule permits).

REFERENCES

[1] Draper, R.F (1988), "The Mariner Mark II Program," Proc. of AIAA Conference, held in Reno, Nevada, January 1988, #880067

[2] Schock, A., and H. Sooklazian (1979) "Conceptual Design of the RTG for Solar-Polar Mission," Presented at the 14th Intersociety Energy Conversion Engineering Conference, held in Boston, Massachusetts, August 1979, #799307.

[3] Cockfield, R.D., R.F. Hartman, C.D. Kelly (1980) "RTG Power Sources for International Solar Polar Mission," Proc. of the 15th Intersociety Energy Conversion Engineering Conference, held in Seattle, Washington, 1980.

[4] Cockfield, R.D. (1986) "Qualification of GPHS-RTG for Galileo and Ulysses," Proc. of the 21st Intersociety Energy Conversion Engineering Conference, held in San Diego, California, 1986.

[5] Schock, A. (1980) "Design Evolution and Verification of the General Purpose Heat Source", Vol. 2, pages 1032-1042. Proc. of the 15th Intersociety Energy Conversion Engineering Conference, held in Seattle, Washington, 1980.

[6] Ioffe, A. F. (1957) Semiconductor Thermoelements and Thermoelectric Cooling Inforsearch, London, 1957.

[7] Schock, A., C. T. Or, and E. A. Skrabek (1990) "Thermal and Electrical Analysis of Mars Rover RTGs, and Performance Comparison of Alternative Design Options," Trans. of the Seventh Symposium on Space Nuclear Power Systems, held in Albuquerque, New Mexico, January 1990.

[8] Schock, A., T. Hamrick, and K. Sankarankandath (1990) "Design and Structural Analysis of Mars Rover RTG," Trans. of the Seventh Symposium on Space Nuclear Power Systems, held in Albuquerque, New Mexico, January 1990.

[9] Schock, A., et al. (1989) "Mars Rover RTG Study," FSC-ESD-217/89/450A. Fairchild Space Company, Germantown, Maryland, November 1989.

[10] Loffreda, J. (1982) "Engineering Unit Test Results," PIR-6377. General Electric, Space Division, Philadelphia, Pennsylvania, May 1982.

[11] ITAS: Integrated Thermal Analysis Systems, Analytix Corporation, Timonium, Maryland, 1990.

[12] Gaski, J. (1986) SINDA (System Improved Numerical Differencing Analyzer) version 1.23 from Network Analysis Associate, Fountain Valley, California.

[13] Raag, V. and K.P. McCarron (1973) "Mathematical Model and Computer Program for the Design and Analysis of Silicon-Germanium Air-Vac RTG Degradation," Memorandum #15, Syncal Corporation, Sunnyvale, California, October 1973.

[14] Mowery, A.L. (1975) "Preliminary Power Degradation Report," Interoffice Memorandum to J. Lombardo, U.S. Energy Research and Development Administration, Washington, D.C., May 1975.

[15] Jet Propulsion Laboratory (1989), D-3384, "Mariner Mark II, Comet Rendezvous and Asteroid Flyby and Cassini, Technical Definition and Cost Review", Volume I, May 23, 1989.

Acknowledgment

The author is pleased to acknowledge the support and encouragement of the Department of Energy's Office of Special Application (J. Turi, Director) and the problem definition furnished by JPL's CRAF/Cassini Project Team.